BrHgO• + CO: Analog of OH + CO and reduction path for Hg(II) in the atmosphere

Dorra Khiri,^a Florent Louis,^a Ivan Černušák^b, Theodore S. Dibble ^{c,*}

- a) Université de Lille, CNRS, UMR 8522-PC2A, PhysicoChimie des Processus de Combustion et de l'Atmosphère, 59000 Lille, France
- b) Department of Physical and Theoretical Chemistry, Faculty of Natural Sciences, Comenius University in Bratislava, Ilkovičova 6, 84215 Bratislava, Slovakia
- c) Department of Chemistry, State University of New York, College of Environmental Science and Forestry, 1 Forestry Drive, Syracuse, NY, 13210

ABSTRACT

We present results of the first study of the reaction $BrHgO^{\bullet} + CO \rightarrow BrHg^{\bullet} + CO_2$, which constitutes a potentially important mercury reduction reaction in the atmosphere. We characterized the potential energy surface with CCSD(T)/CBS energies (with corrections for relativistic effects) at MP2 geometries. Master Equation simulations were used to reveal the factors controlling the overall rate constant. Much of the potential energy surface mimics that for the ubiquitous $OH + CO \rightarrow H + CO_2$ reaction, including the entrance channel and binding energies of intermediates. However, the BrHgOCO intermediate is much less stable than HOCO with respect to loss of CO_2 . This leads to ultrafast dissociation of BrHgOCO and prevents its stabilization in air (unlike HOCO). Because of the relatively high rate constant for $BrHgO^{\bullet} + CO$ and the high abundance of CO throughout the troposphere, this reaction could dominate the atmospheric fate of $BrHgO^{\bullet}$. The $BrHg^{\bullet}$ product of this reaction can dissociate to form Hg(0), and Hg(0) is transferred to ecosystems much more slowly than Hg(II) compounds. Therefore, this reaction could significantly slow the transfer of neurotoxic mercury from the atmosphere to ecosystems.

Keywords: quantum chemistry, kinetics, mercury, atmosphere, radicals

*Corresponding Author: tsdibble@esf.edu

1. INTRODUCTION

Mercury is a neurotoxin which is transported globally by the atmosphere.¹ Mercury deposits from the atmosphere to ecosystems most efficiently when it is in the form of Hg(II) compounds.^{2,3} Unfortunately, we are still uncovering major aspects of the redox chemistry of atmospheric mercury.⁴⁻¹¹ This complicates efforts to predict the impact of emissions reductions on the spatial distribution of mercury entry into ecosystems.^{6,12}

It is believed that atomic bromine is the major agent initiating oxidation of Hg(0). ^{13,10,11,15} Horowitz et al. updated a global model of atmospheric mercury to incorporate recent advancements in the mechanism and kinetics of Hg(0) oxidation by gas-phase Br. ¹³ They found oxidation to proceed so rapidly as to under-predict [Hg(0)], which inspired a search for reduction pathways to add to models. While recent work suggested fast photo-reduction pathways for Hg(I) and Hg(II) compounds, ^{7,16,17} the present work suggests a thermal reaction that could efficiently reduce Hg(II) to Hg(I), namely, the reaction of BrHgO• with CO to produce BrHg• + CO₂.

The Br-initiated oxidation of Hg(0) proceeds via the reversible addition of Br to Hg: 13,18

$$Br^{\bullet} + Hg + M = BrHg^{\bullet} + M$$
 (1)

where M is a third body. BrHg• reacts with other radicals (•Y) in the atmosphere to form Hg(II) compounds: 19,20

$$BrHg \bullet + \bullet Y + M \rightarrow BrHgY + M$$
 (2)

Because NO₂ is the most abundant radical in the atmosphere, BrHg• mostly reacts with NO₂, and the major product of this reaction is BrHgONO.^{11,13,21} Calculations by Francés-Monerris et al.⁷ and Lam et al.²² indicate that BrHgONO can absorb light at $\lambda > 300$ nm. As the flux of such light is relatively intense in the lowermost atmosphere, these groups argued that BrHgONO undergoes fast photolysis. Lam et al.²² and Francés-Monerris et al.⁷ presented evidence that BrHgONO photolysis will mostly produce BrHgO• via:

$$BrHgONO + hv \rightarrow BrHgO \cdot + NO$$
 (3)

BrHgO• is stable with respect to thermal dissociation. 23 Lam et al. 22,24 further showed that the reactivity of BrHgO• in the atmosphere mimics that of the ubiquitous OH radical. Specifically, they found that, like OH, BrHgO• efficiently abstracts hydrogen atoms from alkanes, adds to sp^2 -hybridized carbon atoms of alkenes, and forms bonds with NO and NO2. Inspired by these similarities and the importance of the reaction OH + CO in the chemistry of the terrestrial 25,26 and Martial atmospheres, 27 combustion, $^{28-30}$ and the interstellar medium, 31 we decided to investigate the reaction of BrHgO• with CO:

$$BrHgO \bullet + CO \rightarrow BrHg \bullet + CO_2$$
 (4)

Immediately below we discuss the methods used to characterize this reaction. Next, we discuss the structures and energetics of reaction intermediates and products. We find that reaction (4), like OH + CO, proceeds via XO + CO \Rightarrow XO--CO \rightarrow XOCO \rightarrow X + CO₂ where X= BrHg or H. We then investigate the kinetics of this reaction. Next, we compare and contrast

the energetics and kinetics of BrHgO• + CO with the frequently studied OH + CO system. Finally, we consider the implications of this reaction to mercury redox chemistry in the atmosphere.

2. COMPUTATIONAL METHODS

Dunning's aug-cc-pVTZ basis sets were used for C and O atoms.³² ³³ To account for scalar relativistic effects in Hg and Br, we used the Stuttgart/Cologne scalar pseudopotentials for the 60 innermost electrons of Hg (ECP60MDF) and the 10 innermost electrons of Br (ECP10MDF).^{34,35,36} Structures and harmonic vibrational frequencies of all species were computed using second-order Møller-Plesset perturbation theory (MP2) in Gaussian16.³⁷ These calculations used the spin-unrestricted formalism. We used the corresponding aug-cc-pVTZ(-PP) basis sets of Peterson and co-workers for electrons treated explicitly.^{3,36,38} The combination is henceforth denoted aVTZ. The frozen-core approximation correlated only the 5d and 6s electrons of Hg, the 4s and 4p electrons of Br, and the valence electrons of C and O. Vibrational frequencies were scaled by 0.953 for computing zero-point energies (ZPE).³⁹ Vibrational frequencies were inspected to verify that minima and transition states had the correct number of imaginary vibrational frequencies. Intrinsic reaction coordinate calculations were carried out to verify the identity of transition states.

Single-point CCSD(T) energies were computed in MOLPRO.⁴⁰ Calculations on radicals used UCCSD(T) with ROHF wavefunctions.^{41,42} We used the aug-cc-pwCVnZ (n = D, T, Q, 5) basis sets for C and O atoms.⁴³ Br and Hg atoms were treated by the corresponding aug-cc-pwCVnZ-PP (n = D, T, Q, 5) basis sets of Peterson and co-workers.^{38,44} This basis set is denoted awCVnZ throughout this paper. CCSD(T) energies were extrapolated to the basis set limit using the average of two extrapolations: a two-point extrapolation of the energies at awCVQZ and awCV5Z,⁴⁵ and a three-point extrapolation of the energies at awCVTZ, awCVQZ, and awCV5Z.⁴⁶ The difference between these two extrapolations was less than 1 kJ/mole in relative energy. Corrections for effects of residual core-valence correlation on relative energies (Δ CV) were computed at CCSD(T) using the aug-cc-pwCVTZ(-PP) basis set. The core-valence contribution is taken as the difference energy between the valence electron correlation calculation and that with the nearest core electrons included (1s² for C and O atoms, 3s² 3p⁶ 3d¹⁰ for Br atom, and 5s² 5p⁶ for Hg atom.

Pseudo-potential correction (ΔPP) using the CCSD(T)/aug-cc-pwCVTZ-DK result and the following formula: $\Delta E_{PP} = \Delta E_{aug\text{-}cc\text{-}pw\text{CVTZ-DK}} - (\Delta E_{aug\text{-}cc\text{-}pw\text{CVTZ(-PP)}} + \Delta E_{SR})$. Spin-orbit corrections (ΔSO) were computed with the RASSCF/CASPT2/RASSI^{47,48,49} approach using the ANO-RCC-VTZP basis set. For complexes and transition states the active space comprised 15 electrons in 13 orbitals: 11 electrons in 12 orbitals for BrHgO and 7 electrons in 8 orbitals for BrHg. The RASSI calculation treated the interaction of all states within 6 eV of the ground state: 18 for BrHgO, 12 for HgBr and 10 for the transition states and molecular complexes. The $^2\Pi_{3/2}$ - $^2\Pi_{1/2}$ splitting we compute for BrHgO (520 cm⁻¹) closely matches that computed previously by Balabanov and Peterson (\sim 500 cm⁻¹). 52

The final level of theory is denoted as CCSD(T)/CBS + Δ CV + Δ SO + Δ E_{PP} + Δ ZPE. We have applied this approach previously in a series of papers on atmospheric reactivity of halohydrocarbons^{53–55} and a similar approach in previous work on mercury compounds.⁵⁶ The counterpoise correction for the estimation of the basis set superposition error was not taken into account because several previous works showed that it could lead to discrepancies in the energetic results.^{57–59}

RRKM/Master Equation calculations were carried out in MultiWell^{60–62} using the rigid-rotor/harmonic oscillator approximation. To approximate the effects of conservation of angular momentum on calculations of microcanonical rate constants, k(E), we used the separable rotors approximation. In this treatment, the near-symmetric 2-D rotor was treated as inactive while the 1-D K-rotor contributed to the sums and densities of states. For collisional energy transfer, the bath gas was treated using Lennard-Jones parameters for N₂. The value of the Lennard-Jones ϵ and σ for HgBrCO₂ species was estimated following the guidance from Gilbert and Smith.; specifically, we used the boiling points of HgCl₂ and HgBr₂⁶³ to estimate $\epsilon/k_B = 700$ K and volume additivity considerations^{64,65} to estimate $\sigma = 5.0$ Ångstroms.

3. RESULTS AND DISCUSSION

3.1 Quantum Chemistry Results Here we summarize the mechanism of the reaction of BrHgO with CO. These molecules first form a pair of van der Waals complexes, which we label BrHgO—CO and BrHgO—OC. In the former, the radical center of BrHgO• interacts with the carbon atom of CO, while in the latter it is the oxygen atom of CO that interacts with the radical center. BrHgO—CO can react over a submerged barrier to form trans-BrHgOCO. Trans-BrHgOCO can isomerize to cis-BrHgOCO over a low barrier. Both isomers of BrHgOCO easily rearrange to form a T-shaped BrHg—CO₂ complex. This complex will dissociate to BrHg• + CO₂.

Figure 1 depicts the geometries of all potential energy minima, while Figure 2 displays the structures of all transition states. The difference in structure between the two van der Waals complexes accounts for the absence of a saddle point linking BrHgO—OC to BrHgOCO. All species and transition states possess C_s symmetry, except for the transition state linking cis- and trans-BrHgOCO. In going from BrHgOCO conformers to the transition states for their dissociation, the Hg-O distance only increases by 0.10 Ångstroms.

Relative energies are displayed in Figure 3 at the CCSD(T)/CBS + Δ CV + Δ SO + Δ E_{PP} + Δ ZPE level of theory. Unless otherwise specified, all relative energies are at this level of theory. Note that, because of the wide range of energies, the energy axis in Figure 3 is not to scale. To enable the reader to compare the accuracy of different theoretical approaches, Table 1 lists energies at this level of theory along with MP2/aVTZ and CCSD(T)/CBS results. We can see from Table 1 that the MP2 results provide a reliable semi-quantitative guide to the potential energy profile. The CCSD(T)/CBS results fall very close to the final results: the many correction terms change the relative energies by no more than 5 kJ mol⁻¹. While we did not carry out CCSDT or CCSDT(Q) calculations, a study of the analogous OH + CO system found the effect

of correcting CCSD(T)/CBS energies for these terms altered relative energies by less than 2 kJ mol⁻¹.⁶⁶ Values of the T_I diagnostic lie below 0.030 except for BrHg• and one transition state (discussed below). All these facts support the high accuracy of the relative energies we report here.

BrHgO—OC. BrHgO—CO corresponds to a pre-reactive complex. The saddle point connecting it to *trans*-BrHgOCO lies only 1.8 kJ mol⁻¹ above the complex, so the saddle point lies submerged by 6.2 kJ mol⁻¹ with respect to separated reactants. The two BrHgOCO isomers lies 119 kJ mol⁻¹ (trans) and 138 kJ mol⁻¹ (cis) below BrHgO• + CO. The transition state connecting them lies only 16 kJ mol⁻¹ above *trans*-BrHgOCO. The barrier for *trans*-BrHgOCO dissociating to BrHg—CO₂ is quite low (5.8 kJ mol⁻¹). This low barrier is consistent with the very early structure of the transition state. BrHg—CO₂ possesses a bond energy of only 1 kJ mol⁻¹, so it will fall apart quickly under all atmospheric conditions.

As seen in Table 1, we compute the transition state for *cis*-BrHgOCO dissociating to BrHg—CO₂ to lie below the reactant by 8 kJ mol⁻¹ – a non-physical result. The *T_I* diagnostic for this transition is 0.039, which is high enough to begin to worry about effects of strong electron correlation. We suspected that the geometry computed at MP2 might be the cause of this issue, so we re-optimized the geometry of both *cis*-BrHgOCO and this transition state at CCSD. The CCSD geometries closely mimicked those at MP2 (see Figures 1 and 2), so it does not appear that the MP2 geometry is unusually distorted. Efforts to optimize the structure of the transition state at CCSD(T)/aVTZ were unsuccessful, and we found two negative eigenvalues of the Hessian matrix. It remains unclear whether *cis*-BrHgOCO is a minimum on the potential energy surface.

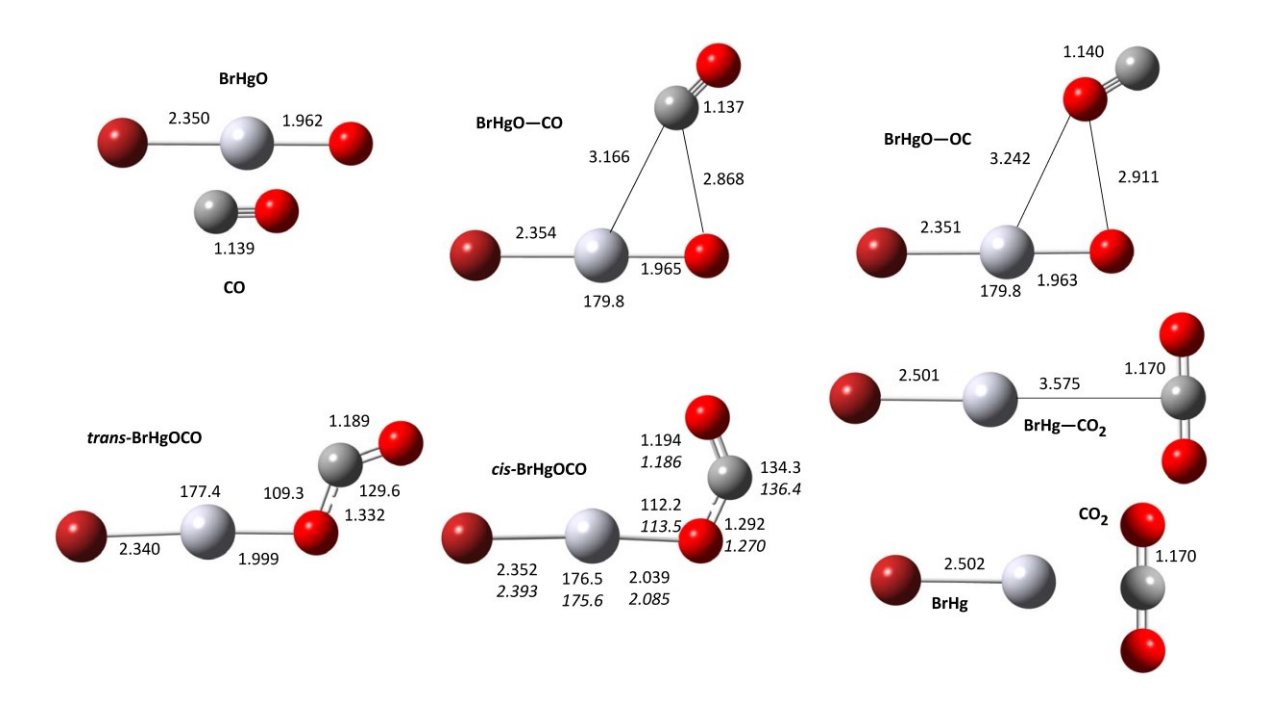


Figure 1. Geometries of all minima (distances in Å, bond angles and dihedral angles in degrees) at MP2/aVTZ (CCSD/aVTZ in italics for one species).

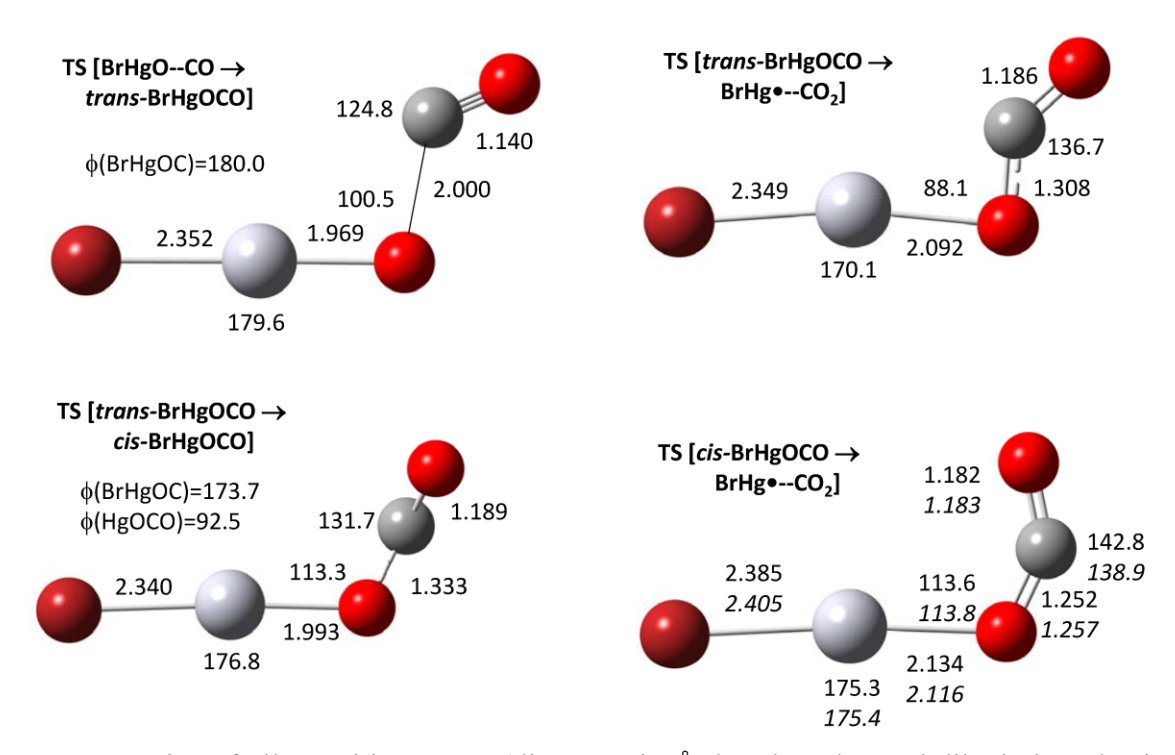


Figure 2. Geometries of all transition states (distances in Å, bond angles and dihedral angles in degrees) at MP2/aVTZ (CCSD/aVTZ in italics for one species).

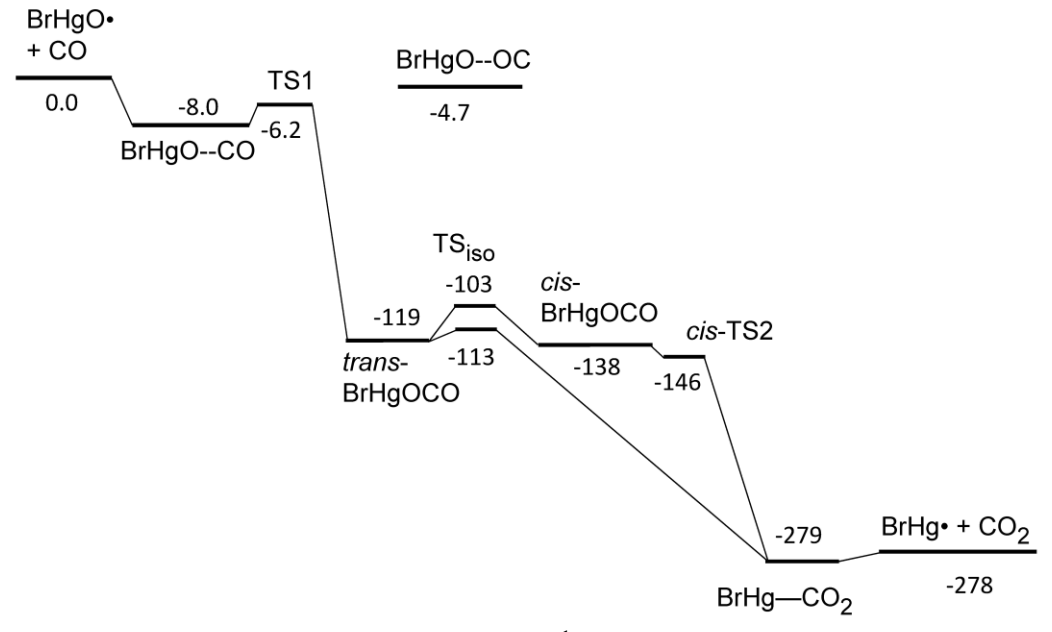


Figure 3. Potential energy profile (kJ mol⁻¹) for BrHgO• + CO at CCSD(T)/CBS + Δ CV + Δ PP + Δ SO + Δ ZPE level of theory.

Table 1. Relative energies (kJ mol⁻¹, including zero-point energy) of reactants, intermediates, products, and transitions states in the BrHgO + CO reaction.

Species	MP2/aVTZ	CCSD(T)/CBS	Final ^a
BrHgO• + CO	0.0	0.0	0.0
BrHgO—CO	-12.0	-9.5	-8.0
TS [BrHgO—CO $\rightarrow trans$ -BrHgOCO] (TS1)	-8.4	-9.9	-6.2
BrHgO—OC	-6.0	-4.8	-4.7
trans-BrHgOCO	-149.3	-121.7	-118.9
cis-BrHgOCO	-157.8	-141.6	-138.2
$TS [trans \rightarrow cis] (TS_{iso})$	-128.7	-105.6	-102.5
TS [trans-BrHgOCO \rightarrow BrHg—CO ₂] (trans-TS2)	-143.5	-116.8	-113.1
TS [cis-BrHgOCO \rightarrow BrHg—CO ₂] (cis-TS2)	-159.1	-146.0	-146.2
BrHg—CO ₂	-317.9	-283.9	-279.3
$BrHg \bullet + CO_2$	-314.0	-282.0	-278.2

a) CCSD(T)/CBS + Δ CV + Δ PP + Δ SO at MP2/AVTZ geometry

3.2 Master Equation Simulations The potential energy surface is very flat in the region of the entrance channel for formation of BrHgO—CO, and our MP2 calculations found extra imaginary frequencies. This probably arises from coupling of translational and/or rotational modes to low-frequency vibrational modes.^{67,68} This precludes using standard variational transition state theory (VTST) to determine the kinetics of the reaction BrHgO• + CO → BrHgO—CO. A variable reaction coordinate VTST approach⁶⁹ would be necessary, but that effort is outside the scope of this study. Here we treated the kinetics of the association reaction using the Inverse LaPlace transform (ILT), and counted BrHgO—CO as a potential energy minimum ("well") in the Master Equation simulations.

To use the ILT method, one must assume a value for A_{∞} , the Arrhenius pre-exponential factor in the high-pressure limit for dissociation of BrHgO—CO to reactants. We considered values of 10^{13} and 10^{14} s⁻¹ to see their impact on predicted rate constants. Master Equation simulations neglected BrHgO—OC, as it does not appear to play a role in the reaction. We also neglected the exit channel complex BrHg—CO₂.

Simulations started with population in the BrHgO—CO well, and ran for ~20 ps at a total pressure of N₂ bath gas of 0.01, 0.1, and 1.0 atm. At the end of the simulation, all the population had been transferred from BrHgO—CO to either separated BrHgO + CO or BrHg + CO₂. We estimated the effective 2^{nd} -order rate constants, k(P,T), from:

$$k(P,T) = f(P,T) \times k_{\text{collision}}$$
 (5)

where f(P,T) corresponds to the fraction of collisions leading to BrHg• + CO₂ and $k_{\text{collision}}$ is the collision rate constant. We carried out 10^7 Monte Carlo trials to obtain better than 1% precision in f(P,T). We used a value of $k_{\text{collision}}$ of 2×10^{10} cm³ molecule⁻¹ s⁻¹. Table 2 shows the values of f at 200 and 298 K as a function of A_{∞} .

Table 2. Fraction, f, of BrHgO—CO going on to form BrHg• + CO₂, and overall rate constant, k(P,T), for BrHgO• + CO \rightarrow BrHg• + CO₂, at 200 and 298 K and a pressure of 1 atm.

T(K)	A_{∞} (s ⁻¹)	f	$k \text{ (cm}^3 \text{ molecule}^{-1} \text{ s}^{-1})$
200	10^{13}	0.143	2.9×10^{-11}
	10^{14}	0.019	3.8×10^{-12}
298	10^{13}	0.262	5.2×10^{-11}
_, _,	10^{14}	0.047	9.4×10^{-12}

As can be seen from Table 2, the fraction reacting, and, consequently, the overall rate constant, k(T), depends rather sensitively on the assumed value of A_{∞} . This resulting uncertainty in k(T) makes it pointless to worry about the temperature dependence of, or uncertainty in, $k_{\text{collision}}$. The fraction reacting varies by less than 5% when the simulated pressure rises from 0.01 atm to 1 atm. The dissociation of cis-BrHgOCO was assumed to have a barrier of 1 kJ mol⁻¹; a value as high as 40 kJ mol⁻¹ changed the fraction reacting by no more than 3%. A second set of simulations was carried out while initially populating *trans*-BrHgOCO with internal energy equivalent to being formed from separated BrHgO• + CO. Dissociation of BrHgOCO to BrHg• +

CO₂ was 90% complete in 1 ps, and even when BrHgOCO was given 30 kJ mol⁻¹ of energy above that of reactants, only 0.2% back-reacted to BrHgO• + CO.

3.3 Comparison to OH + CO It is interesting to compare the potential energy profiles and kinetics of BrHgO• + CO to those of OH + CO. Figure 4 displays the potential energy profile for OH + CO based on the HEAT-345(Q) energies reported by Lam and co-workers. ⁶⁶ This method provides CCSDT(Q) energies based on geometries computed at CCSD(T)/cc-pVQZ. Both systems possess XO•—CO and XO•—OC van der Waals complexes where the XO—CO complex is more strongly bound than XO•—OC. The barrier from BrHgO—CO to *trans*-BrHgOCO lies 6 kJ mol⁻¹ below separated reactants, whereas the barrier from HO—CO to *trans*-HOCO lies 4 kJ mol⁻¹ above the reactants. BrHgOCO is more strongly bound than HOCO by ~15 kJ mol⁻¹ for the trans isomer and ~40 kJ mol⁻¹ for the cis isomer. The major difference between the two systems is that the reaction BrHgO• + CO \rightarrow BrHg• + CO₂ is exothermic by 280 kJ mol⁻¹, while OH + CO \rightarrow H + CO₂ is only exothermic by 103 kJ mol⁻¹.

The first consequence of the large stability of BrHg• + CO₂ with respect to BrHgO• + CO is that the barriers for BrHgOCO \rightarrow BrHg• + CO₂ are very low, while that for HOCO \rightarrow H• + CO₂ is substantial (~120 kJ mol⁻¹). Note that the barriers to for the reverse reactions (X + CO₂ \rightarrow XOCO) are large for both X = H and X = BrHg (~120 and ~170 kJ mol⁻¹). The second consequence is that the BrHgCO₂ analogue of the HCO₂ molecule is a van der Waals complex, rather than a molecule with an activation barrier of ~50 kJ mol⁻¹ with respect to dissociation.

A consequence of the high barrier separating HOCO from H + CO₂ is that *cis*- and *trans*-HOCO can be stabilized under atmospheric conditions.^{26,70} In fact, these intermediates have been observed in the gas phase.^{70,71} By contrast, our RRKM/ME simulations indicate that BrHgOCO dissociates before it could even undergo one stabilizing collision with bath gas.

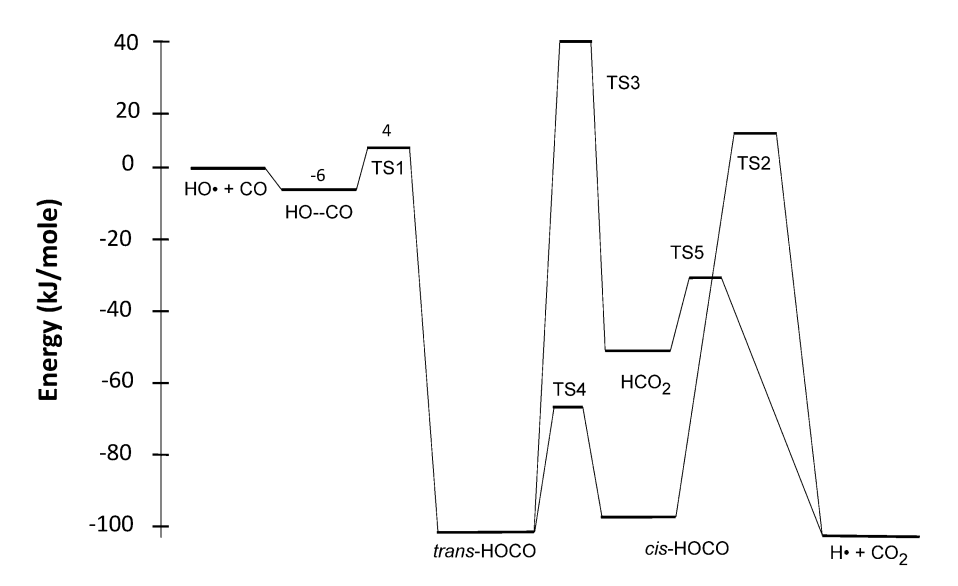


Figure 4. Potential energy profile (kJ mol⁻¹) for BrHgO• + CO at the HEAT composite level of theory.⁶⁶

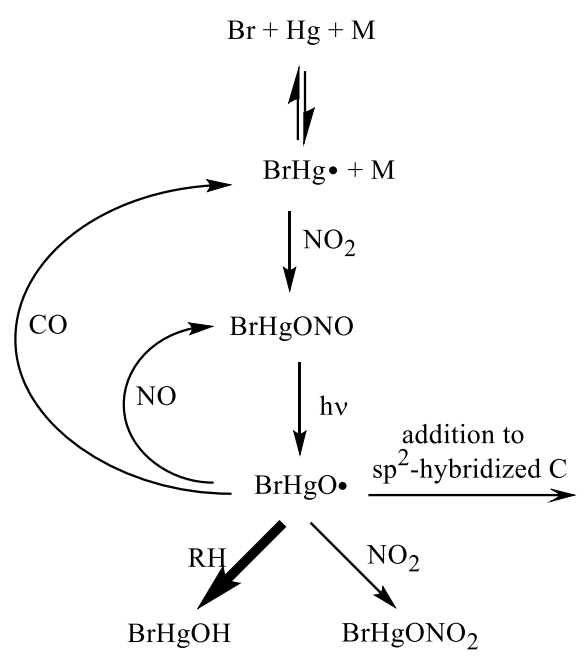
We note, in passing, the major difference between the reactions of BrHgO• and OH with CO and the reaction CH₃O• + CO. Reaction of CH₃O• with CO to make CH₃ + CO₂ (Δ_r H° = 158 kJ mol⁻¹)^{72,73} is somewhat more exothermic than OH + CO \rightarrow H + CO₂, but has a much larger entrance channel barrier than its analogs (25 kJ/mole).⁷⁴

3.4 Implications for Mercury Redox Cycling in the Atmosphere

BrHg• produced in the reaction BrHgO• + CO \rightarrow BrHg• + CO₂ can dissociate in competition with bimolecular reactions to make Hg(II) compounds. ^{19,20} The larger the fraction of BrHgO• reacting with CO, the longer the residence time of mercury in the atmosphere and the greater the extent of mercury deposition as Hg(0) rather than Hg(II) compounds. Previous work by Lam et al. mapped out most competing types of reactions of BrHgO•. ^{22,24} Scheme 1 depicts their results together with the findings of this work. BrHgO• is very effective at abstracting hydrogen atoms from sp³-hybridized carbon atoms, and this reaction dominated the fate of BrHgO• in the analysis of Lam et al. The model reaction:

$$BrHgO \bullet + CH_4 \rightarrow BrHgOH + \bullet CH_3$$
 (6)

was computed to proceed with a pseudo-1st order rate constant (at [CH₄] = 1.85 ppmv) of 11 s⁻¹ at 298 K and 1 atm. Given typical values of [CO] of 60-120 ppbv, the corresponding pseudo-1st order rate constant for reaction of BrHgO• with CO would range from 14 – 150 s⁻¹, depending largely on the assumed value of A_{∞} in Table 2.



Scheme 1. Reactions forming BrHgO via BrHg + NO₂ and removing BrHgO•.

The analysis above applies near ground level. Concentrations of both mercury and CO tend to be higher in the Northern Hemisphere than the Southern Hemisphere, which tends to increase the potential importance of the BrHgO• + CO reaction. In fact, the IAGOS-CARABIC observatory finds the peaks of [CO] and the concentration of total gaseous mercury in the troposphere to be nearly co-located in space and time.⁷⁵ The analysis in the previous paragraph also neglects other potential molecules from which BrHgO• can abstract hydrogen atoms. Unfortunately, rate constants for hydrogen abstraction by BrHgO• are not available for a wide range of potential reactants. However, reaction with CO is a significant fate of OH radical in much of the atmosphere, ^{76–78} so it seems reasonable to suppose that this is also true of BrHgO•.

4. CONCLUSIONS AND FURTHER WORK

We have mapped out the potential energy surface for BrHgO• reacting with CO. This reaction corresponds to reducing Hg(II) to Hg(I). The rate of this reaction may outcompete all other reactions of BrHgO• in the atmosphere at 298 K and 1 atm, and likely contributes significantly to the loss rate of BrHgO• in much of the global troposphere. The major fate of BrHg is to react with NO₂, and the product of this reaction mostly undergoes photolysis to make BrHgO•. Consequently, the title reaction could have a large impact on mercury redox chemistry in the atmosphere. The factor of ~10 uncertainty in the computed rate constant for this reaction could propagate to significant uncertainties in our understanding of atmospheric mercury chemistry.

The rate-limiting step in the title reaction appears to be the rearrangement of the pre-reactive complex to *trans*-BrHgOCO. The formation and fate of this pre-reactive complex requires further study in order to determine the overall rate constant for reaction. While ordinarily one would prefer to rely on experimentally measured rate constants, the complete absence of experimental data on BrHgO• dims the prospects for such measurements.

As can be seen from Figure 3, the BrHgO• + CO \rightarrow BrHg• + CO₂ reaction is exothermic by 282 kJ mol⁻¹. The bond energy of BrHg is only 65 kJ mol⁻¹,^{79,80} so some fraction of chemically activated BrHg• formed in this reaction may possess sufficient energy to promptly dissociate to Br + Hg. To investigate this phenomenon would require carrying out molecular dynamics simulations using either a reactive potential energy surface or computing internuclear forces on the fly.

It is conceivable that BrHgOCO could be stabilized in cryogenic matrices. To aid the detection of BrHgOCO, we have reported vibrational frequencies and intensities in the Supporting Information.

■ ASSOCIATED CONTENT

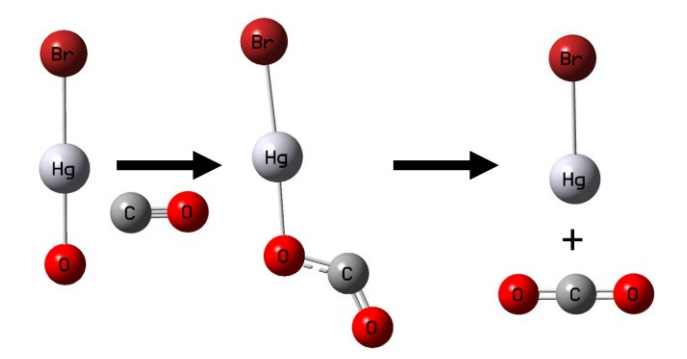
Supporting Information

The Supporting Information is available free of charge on the ACS Publications website at DOI: ____. Absolute energies of all species at all levels of theory along with zero-point energies, Cartesian coordinates, rotational constants, and vibrational frequencies; values of the T1 diagnostic; images of orbitals used in RASSCF/CASPT2/RASSI calculations of Δ SO (XLS).

ACKNOWLEDGEMENTS

Neal M. Donahue first suggested that we investigate BrHgO• + CO. This work was part of the CaPPA project (Chemical and Physical Properties of the Atmosphere), which is funded by the French National Research Agency (ANR) through the PIA (Programme d'Investissement d'Avenir) under contract "ANR-11-LABX-0005-01" and by the Regional Council "Nord-Pas de Calais" and the "European Funds for Regional Economic Development". IČ thanks Slovak Research and Development Agency (project APVV-15-0105) and VEGA (grant 1/0777/19) for funding. Work at Comenius University was supported in part through the high performance computing facilities, services and staff expertise of Centre for Information Technology (https://uniba.sk/en/HPC-Clara). Work at SUNY-ESF was supported by the United States National Science Foundation under award 1609848. We thank three anonymous reviewers for their extensive comments which helped us strengthen this manuscript.

TOC Graphic



REFERENCES

- (1) Driscoll, C. T.; Mason, R. P.; Chan, H. M.; Jacob, D. J.; Pirrone, N. Mercury as a Global Pollutant: Sources, Pathways, and Effects. *Environ. Sci. Technol.* **2013**, *47* (10), 4967–4983. https://doi.org/10.1021/es305071v.
- (2) Cheng, I.; Zhang, L.; Blanchard, P.; Graydon, J. A.; St. Louis, V. L. Source-Receptor Relationships for Speciated Atmospheric Mercury at the Remote Experimental Lakes Area, Northwestern Ontario, Canada. *Atmos. Chem. Phys.* **2012**, *12* (4), 1903–1922. https://doi.org/10.5194/acp-12-1903-2012.
- (3) Zhang, L.; Zhou, P.; Cao, S.; Zhao, Y. Atmospheric Mercury Deposition over the Land Surfaces and the Associated Uncertainties in Observations and Simulations: A Critical Review. *Atmos. Chem. Phys.* **2019**, *19* (24), 15587–15608. https://doi.org/10.5194/acp-19-15587-2019.
- (4) Lyman, S. N.; Cheng, I.; Gratz, L. E.; Weiss-Penzias, P.; Zhang, L. An Updated Review of Atmospheric Mercury. *Sci. Total Environ.* **2019**, 707, 135575. https://doi.org/10.1016/j.scitotenv.2019.135575.
- (5) Timonen, H.; Ambrose, J. L.; Jaffe, D. A. Oxidation of Elemental Hg in Anthropogenic and Marine Airmasses. *Atmos. Chem. Phys.* **2013**, *13* (5), 2827–2836. https://doi.org/10.5194/acp-13-2827-2013.
- (6) Travnikov, O.; Angot, H.; Artaxo, P.; Bencardino, M.; Bieser, J.; D'Amore, F.; Dastoor, A.; De Simone, F.; Diéguez, M. del C.; Dommergue, A.; Ebinghaus, R.; Feng, X. Bin; Gencarelli, C. N.; Hedgecock, I. M.; Magand, O.; Martin, L.; Matthias, V.; Mashyanov, N.; Pirrone, N.; Ramachandran, R.; Read, K. A.; Ryjkov, A.; Selin, N. E.; Sena, F.; Song, S.; Sprovieri, F.; Wip, D.; Wängberg, I.; Yang, X. Multi-Model Study of Mercury Dispersion in the Atmosphere: Atmospheric Processes and Model Evaluation. *Atmos. Chem. Phys.* 2017, 17 (8), 5271–5295. https://doi.org/10.5194/acp-17-5271-2017.
- (7) Francés-Monerris, A.; Carmona-García, J.; Acuña, A. U.; Dávalos, J. Z.; Cuevas, C. A.; Kinnison, D. E.; Francisco, J. S.; Saiz-Lopez, A.; Roca-Sanjuán, D. Photodissociation Mechanisms of Major Mercury(II) Species in the Atmospheric Chemical Cycle of Mercury. *Angew. Chemie Int. Ed.* **2020**, *59*, 2–8. https://doi.org/10.1002/anie.201915656.
- (8) Song, S.; Selin, N. E.; Soerensen, A. L.; Angot, H.; Artz, R.; Brooks, S.; Brunke, E.-G.; Conley, G.; Dommergue, A.; Ebinghaus, R.; Holsen, T. M.; Jaffe, D. A.; Kang, S.; Kelley, P.; Luke, W. T.; Magand, O.; Marumoto, K.; Pfaffhuber, K. A.; Ren, X.; Sheu, G.-R.; Slemr, F.; Warneke, T.; Weigelt, A.; Weiss-Penzias, P.; Wip, D. C.; Zhang, Q. Top-down Constraints on Atmospheric Mercury Emissions and Implications for Global Biogeochemical Cycling. *Atmos. Chem. Phys.* **2015**, *15* (12), 7103–7125. https://doi.org/10.5194/acp-15-7103-2015.
- (9) Dibble, T. S.; Tetu, H. L.; Jiao, Y.; Thackray, C. P.; Jacob, D. J. Modeling the OH-Initiated Oxidation of Mercury in the Global Atmosphere without Violating Physical Laws. *J. Phys. Chem. A* **2020**, *124* (2), 444–453. https://doi.org/10.1021/acs.jpca.9b10121.
- (10) Coburn, S.; Dix, B.; Edgerton, E.; Holmes, C. D.; Kinnison, D.; Liang, Q.; ter Schure, A.; Wang, S.; Volkamer, R. Mercury Oxidation from Bromine Chemistry in the Free

- Troposphere over the Southeastern US. *Atmos. Chem. Phys.* **2016**, *16* (6), 3743–3760. https://doi.org/10.5194/acp-16-3743-2016.
- (11) Wu, R.; Wang, C.; Dibble, T. S. First Experimental Kinetic Study of the Atmospherically Important Reaction of BrHg• + NO₂. *Chem. Phys. Lett.* **2020**. https://doi.org/10.1016/j.cplett.2020.137928.
- (12) Ye, Z.; Mao, H.; Driscoll, C. T.; Wang, Y.; Zhang, Y.; Jaeglé, L. Evaluation of CMAQ Coupled With a State-of-the-Art Mercury Chemical Mechanism (CMAQ-newHg-Br). *J. Adv. Model. Earth Syst.* **2018**, *10* (3), 668–690. https://doi.org/10.1002/2017MS001161.
- (13) Goodsite, M. E. Plane, J. M. C.; Skov, H. A Theoretical Study of the Oxidation of Hg0 to HgBr2 in the Troposphere. *Environ. Sci. Technol.* **2004**, *38* (6), 1772–1776. https://doi.org/10.1021/es034680s.
- (14) Calvert, J. G.; Lindberg, S. E. Mechanisms of Mercury Removal by O₃ and OH in the Atmosphere. *Atmos. Environ.* **2005**, *39* (18), 3355–3367. https://doi.org/10.1016/j.atmosenv.2005.01.055.
- (15) Cremer, D.; Kraka, E.; Filatov, M. Bonding in Mercury Molecules Described by the Normalized Elimination of the Small Component and Coupled Cluster Theory. *Chemphyschem* **2008**, *9* (17), 2510–2521. https://doi.org/10.1002/cphc.200800510.
- (16) Saiz-Lopez, A.; Sitkiewicz, S. P.; Roca-Sanjuán, D.; Oliva-Enrich, J. M.; Dávalos, J. Z.; Notario, R.; Jiskra, M.; Xu, Y.; Wang, F.; Thackray, C. P.; Sunderland, E. M.; Jacob, D. J.; Travnikov, O.; Cuevas, C. A.; Acuña, A. U.; Rivero, D.; Plane, J. M. C.; Kinnison, D. E.; Sonke, J. E. Photoreduction of Gaseous Oxidized Mercury Changes Global Atmospheric Mercury Speciation, Transport and Deposition. *Nat. Commun.* 2018, 9 (1), 4796. https://doi.org/10.1038/s41467-018-07075-3.
- (17) Saiz-Lopez, A.; Ulises Acuña, A.; Trabelsi, T.; Carmona-García, J.; Z. Dávalos, J.; Rivero, D.; A. Cuevas, C.; E. Kinnison, D.; P. Sitkiewicz, S.; Roca-Sanjuán, D.; S. Francisco, J. Gas-Phase Photolysis of Hg(I) Radical Species: A New Atmospheric Mercury Reduction Process. *J. Am. Chem. Soc.* 2019, 141 (22), 8698–8702. https://doi.org/10.1021/jacs.9b02890.
- (18) Donohoue, D. L.; Bauer, D.; Cossairt, B.; Hynes, A. J. Temperature and Pressure Dependent Rate Coefficients for the Reaction of Hg with Br and the Reaction of Br with Br: A Pulsed Laser Photolysis-Pulsed Laser Induced Fluorescence Study. *J. Phys. Chem. A* **2006**, *110*, 6623–6632. https://doi.org/10.1021/JP054688J.
- (19) Dibble, T. S.; Zelie, M. J.; Mao, H. Thermodynamics of Reactions of ClHg and BrHg Radicals with Atmospherically Abundant Free Radicals. *Atmos. Chem. Phys.* **2012**, *12* (21), 10271–10279. https://doi.org/10.5194/acp-12-10271-2012.
- (20) Horowitz, H. M.; Jacob, D. J.; Zhang, Y.; Dibble, T. S.; Slemr, F.; Amos, H. M.; Schmidt, J. A.; Corbitt, E. S.; Marais, E. A.; Sunderland, E. M. A New Mechanism for Atmospheric Mercury Redox Chemistry: Implications for the Global Mercury Budget. *Atmos. Chem. Phys.* **2017**, *17*, 6353–6371. https://doi.org/10.5194/acp-17-6353-2017.
- (21) Jiao, Y.; Dibble, T. S. First Kinetic Study of the Atmospherically Important Reactions

- BrHg + NO₂ and BrHg + HOO. *Phys. Chem. Chem. Phys.* **2017**, *19* (3), 1826–1838. https://doi.org/10.1039/c6cp06276h.
- (22) Lam, K. T.; Wilhelmsen, C. J.; Schwid, A. C.; Jiao, Y.; Dibble, T. S. Computational Study on the Photolysis of BrHgONO and the Reactions of BrHgO• with CH₄, C₂H₆, NO, and NO₂: Implications for Formation of Hg(II) Compounds in the Atmosphere. *J. Phys. Chem. A* **2019**, *123* (8), 1637–1647. https://doi.org/10.1021/acs.jpca.8b11216.
- (23) Balabanov, N. B.; Peterson, K. A. Mercury and Reactive Halogens: The Thermochemistry of Hg + {Cl 2, Br2, BrCl, ClO, and BrO}. *J. Phys. Chem. A* **2003**, *107* (38), 7465–7470. https://doi.org/10.1021/jp035547p.
- (24) Lam, K. T.; Wilhelmsen, C. J.; Dibble, T. S. BrHgO• + C2H4 and BrHgO• + HCHO in Atmospheric Oxidation of Mercury: Determining Rate Constants of Reactions with Pre-Reactive Complexes and a Bifurcation. *J. Phys. Chem. A* **2019**, *123*, 6045–6055. https://doi.org/10.1021/acs.jpca.9b05120.
- (25) Nölscher, A. C.; Yañez-Serrano, A. M.; Wolff, S.; De Araujo, A. C.; Lavrič, J. V.; Kesselmeier, J.; Williams, J. Unexpected Seasonality in Quantity and Composition of Amazon Rainforest Air Reactivity. *Nat. Commun.* **2016**, *7* (1), 1–12. https://doi.org/10.1038/ncomms10383.
- (26) Liu, Y.; Sander, S. P. Rate Constant for the OH + CO Reaction at Low Temperatures. *J. Phys. Chem. A* **2015**, *119* (39), 10060–10066. https://doi.org/10.1021/acs.jpca.5b07220.
- (27) Boxe, C. S.; Francisco, J. S.; Shia, R. L.; Yung, Y. L.; Nair, H.; Liang, M. C.; Saiz-Lopez, A. New Insights into Martian Atmospheric Chemistry. *Icarus* **2014**, *242*, 97–104. https://doi.org/10.1016/j.icarus.2014.07.023.
- (28) Nilsson, E. J. K.; Konnov, A. A. Role of HOCO Chemistry in Syngas Combustion. *Energy and Fuels* **2016**, *30* (3), 2443–2457. https://doi.org/10.1021/acs.energyfuels.5b02778.
- (29) Mathieu, O.; Mulvihill, C. R.; Petersen, E. L. Assessment of Modern Detailed Kinetics Mechanisms to Predict CO Formation from Methane Combustion Using Shock-Tube Laser-Absorption Measurements. *Fuel* **2019**, *236*, 1164–1180. https://doi.org/10.1016/j.fuel.2018.09.029.
- (30) Bjork, B. J.; Bui, T. Q.; Heckl, O. H.; Changala, P. B.; Spaun, B.; Heu, P.; Follman, D.; Deutsch, C.; Cole, G. D.; Aspelmeyer, M.; Okumura, M.; Ye, J. Direct Frequency Comb Measurement of OD + CO→DOCO Kinetics. *Science* **2016**, *354* (6311), 444–448. https://doi.org/10.1126/science.aag1862.
- (31) Noble, J. A.; Dulieu, F.; Congiu, E.; Fraser, H. J. CO₂ Formation in Queiscent Clouds: An Experimental Study of the CO + OH Pathway. *Astrophys. J.* **2011**, 735 (2), 121. https://doi.org/10.1088/0004-637X/735/2/121.
- (32) Peterson, K. A.; Dunning, T. H. Accurate Correlation Consistent Basis Sets for Molecular Core–Valence Correlation Effects: The Second Row Atoms Al–Ar, and the First Row Atoms B–Ne Revisited. *J. Chem. Phys.* **2002**, *117* (23), 10548–10560. https://doi.org/10.1063/1.1520138.

- (33) Dunning, T. H. Gaussian Basis Sets for Use in Correlated Molecular Calculations. I. The Atoms Boron through Neon and Hydrogen. *J. Chem. Phys.* **1989**, *90* (2), 1007–1023. https://doi.org/10.1063/1.456153.
- (34) Peterson, K. A.; Figgen, D.; Goll, E.; Stoll, H.; Dolg, M. Systematically Convergent Basis Sets with Relativistic Pseudopotentials. II. Small-Core Pseudopotentials and Correlation Consistent Basis Sets for the Post-d Group 16–18 Elements. *J. Chem. Phys.* **2003**, *119* (21), 11113. https://doi.org/10.1063/1.1622924.
- (35) Figgen, D.; Rauhut, G.; Dolg, M.; Stoll, H. Energy-Consistent Pseudopotentials for Group 11 and 12 Atoms: Adjustment to Multi-Configuration Dirac-Hartree-Fock Data. *Chem. Phys.* **2005**, *311* (1–2), 227–244. https://doi.org/10.1016/j.chemphys.2004.10.005.
- (36) Peterson, K. A.; Shepler, B. C.; Figgen, D.; Stoll, H. On the Spectroscopic and Thermochemical Properties of ClO, BrO, IO, and Their Anions. *J. Phys. Chem. A* **2006**, 110 (51), 13877–13883. https://doi.org/10.1021/jp0658871.
- (37) Frisch, M. J.; Trucks, G. W.; Schlegel, H. B.; Scuseria, G. E.; Robb, M. A.; Cheeseman, J. R.; Scalmani, G.; Barone, V.; Petersson, G. A.; Nakatsuji, H.; Li, X.; Caricato, M.; Marenich, A. V.; Bloino, J.; Janesko, B. G.; Gomperts, R.; Mennucci, B.; Hratch, D. J. Gaussian 16, Rev. A. Gaussian, Inc.: Wallingford CT 2016.
- (38) Peterson, K. A.; Puzzarini, C. Systematically Convergent Basis Sets for Transition Metals. II. Pseudopotential-Based Correlation Consistent Basis Sets for the Group 11 (Cu, Ag, Au) and 12 (Zn, Cd, Hg) Elements. *Theor. Chem. Acc.* **2005**, *114* (4–5), 283–296. https://doi.org/10.1007/s00214-005-0681-9.
- (39) Johnson, R. D. I. NIST Computational Chemistry Comparison and Benchmark Database. 2015. https://doi.org/10.18434/T47C7Z.
- (40) H.-J. Werner, P. J. Knowles, G. Knizia, F. R. Manby, M. Schütz, P. Celani, W. Györffy, D. Kats, T. Korona, R. Lindh, A. Mitrushenkov, G. Rauhut, K. R. Shamasundar, T. B. Adler, R. D. Amos, S. J. Bennie, A. Bernhardsson, A. Berning, D. L. Cooper, M. J. O., and M. W. MOLPRO, Version 2019.1, a Package of Ab Initio Programs. 2019.
- (41) Knowles, P. J.; Hampel, C.; Werner, H. Coupled Cluster Theory for High Spin, Open Shell Reference Wave Functions. *J. Chem. Phys.* **1993**, *99* (7), 5219–5227. https://doi.org/10.1063/1.465990.
- (42) Knowles, P. J.; Hampel, C.; Werner, H.-J. Erratum: "Coupled Cluster Theory for High Spin, Open Shell Reference Wave Functions" [J. Chem. Phys. **99**, 5219 (1993)]. *J. Chem. Phys.* **2000**, *112* (6), 3106–3107. https://doi.org/10.1063/1.480886.
- (43) Peterson, K. A.; Dunning, T. H. Accurate Correlation Consistent Basis Sets for Molecular Core-Valence Correlation Effects: The Second Row Atoms Al-Ar, and the First Row Atoms B-Ne Revisited. *J. Chem. Phys.* **2002**, *117* (23), 10548–10560. https://doi.org/10.1063/1.1520138.
- (44) DeYonker, N. J.; Peterson, K. A.; Wilson, A. K. Systematically Convergent Correlation Consistent Basis Sets for Molecular Core-Valence Correlation Effects: The Third-Row Atoms Gallium through Krypton. *J. Phys. Chem. A* **2007**, *111* (44), 11383–11393.

- https://doi.org/10.1021/jp0747757.
- (45) Min, S. K.; Lee, E. C.; Lee, H. M.; Kim, D. Y.; Kim, D.; Kim, K. S. Complete Basis Set Limit of Ab Initio Binding Energies and Geometrical Parameters for Various Typical Types of Complexes. *J. Comput. Chem.* **2008**, *29* (8), 1208–1221. https://doi.org/10.1002/jcc.20880.
- (46) Peterson, K. A.; Woon, D. E.; Dunning, T. H. Benchmark Calculations with Correlated Molecular Wave Functions. IV. The Classical Barrier Height of the H+H2→H₂+H Reaction. *J. Chem. Phys.* **1994**, *100* (10), 7410–7415. https://doi.org/10.1063/1.466884.
- (47) Roos, B. O.; Malmqvist, P. A. Relativistic Quantum Chemistry: The Multiconfigurational Approach. *Phys. Chem. Chem. Phys.* **2004**, *6* (11), 2919–2927. https://doi.org/10.1039/b401472n.
- (48) Ghigo, G.; Roos, B. O.; Malmqvist, P.-Å. A Modified Definition of the Zeroth-Order Hamiltonian in Multiconfigurational Perturbation Theory (CASPT2). *Chem. Phys. Lett.* **2004**, *396* (1–3), 142–149. https://doi.org/10.1016/j.cplett.2004.08.032.
- (49) Malmqvist, P. Å.; Roos, B. O.; Schimmelpfennig, B. The Restricted Active Space (RAS) State Interaction Approach with Spin-Orbit Coupling. *Chem. Phys. Lett.* **2002**, *357* (3–4), 230–240. https://doi.org/10.1016/S0009-2614(02)00498-0.
- (50) Roos, B. O.; Lindh, R.; Malmqvist, P. Å.; Veryazov, V.; Widmark, P. O. Main Group Atoms and Dimers Studied with a New Relativistic ANO Basis Set. *J. Phys. Chem. A* **2004**, *108* (15), 2851–2858. https://doi.org/10.1021/jp031064+.
- (51) Roos, B. O.; Lindh, R.; Malmqvist, P.-Å.; Veryazov, V.; Widmark, P.-O. New Relativistic ANO Basis Sets for Transition Metal Atoms. *J. Phys. Chem. A* **2005**, *109* (29), 6575–6579. https://doi.org/10.1021/JP0581126.
- (52) Balabanov, N. B.; Peterson, K. A. Accurate Theoretical Near-Equilibrium Potential Energy and Dipole Moment Surfaces of HgClO and HgBrO. *J. Chem. Phys.* **2004**, *120* (14), 6585–6592. https://doi.org/10.1063/1.1652435.
- (53) Taamalli, S.; Khiri, D.; Suliman, S.; Khanniche, S.; Černušák, I.; Cantrel, L.; Ribaucour, M.; Louis, F. Unraveling the Tropospheric Microhydration Processes of Iodous Acid HOIO. *ACS Earth Sp. Chem.* **2019**, *4* (1). https://doi.org/10.1021/acsearthspacechem.9b00257.
- (54) Fortin, C.; Khanniche, S.; Khiri, D.; Fèvre-Nollet, V.; Lebègue, P.; Cousin, F.; Černušák, I.; Louis, F. Reactivity of Hydrogen Peroxide with Br and I Atoms. *J. Phys. Chem. A* **2018**, *122* (4), 1053–1063. https://doi.org/10.1021/acs.jpca.7b10318.
- (55) Khiri, D.; Černušák, I.; Louis, F. Theoretical Study of the Reactions of H Atoms with CH₃I and CH₂I₂. *J. Phys. Chem. A* **2018**, *122* (32), 6546–6557. https://doi.org/10.1021/acs.jpca.8b04748.
- (56) Jiao, Y.; Dibble, T. S. Structures, Vibrational Frequencies, and Bond Energies of the BrHgOX and BrHgXO Species Formed in Atmospheric Mercury Depletion Events. *J. Phys. Chem. A* **2017**, *121* (41), 7976–7985. https://doi.org/10.1021/acs.jpca.7b06829.

- (57) Galano, A.; Alvarez–Idaboy, J. R. A New Approach to Counterpoise Correction to BSSE. J. Comput. Chem. **2006**, 27 (11), 1203–1210. https://doi.org/10.1002/jcc.20438.
- (58) Wallnoefer, H. G.; Fox, T.; Liedl, K. R.; Tautermann, C. S. Dispersion Dominated Halogen-π Interactions: Energies and Locations of Minima. *Phys. Chem. Chem. Phys.* 2010, 12 (45), 14941–14949. https://doi.org/10.1039/c0cp00607f.
- (59) Alvarez-Idaboy, J. R.; Galano, A. Counterpoise Corrected Interaction Energies Are Not Systematically Better than Uncorrected Ones: Comparison with CCSD(T) CBS Extrapolated Values. *Theor. Chem. Acc.* **2010**, *126* (1), 75–85. https://doi.org/10.1007/s00214-009-0676-z.
- (60) Barker, J. R.; Nguyen, T. L.; Stanton, J. F.; Aieta, C.; Ceotto, M.; Gabas, F.; Kumar, T. J. D.; Li, C. G. L.; Lohr, L. L.; Maranzana, A.; Ortiz, N. F.; Preses, J. M.; Simmie, J. M.; Sonk, J. A.; Stimac, P. J. MultiWell-2019 Software Suite; J. R. Barker, University of Michigan, Ann Arbor, Michigan, USA, 2019 H.
- (61) Barker, J. R. Multiple-Well, Multiple-Path Unimolecular Reaction Systems. I. MultiWell Computer Program Suite. *Int. J. Chem. Kinet.* **2001**, *33* (4), 232–245. https://doi.org/10.1002/kin.1017.
- (62) Barker, J. R.; Ortiz, N. F. Multiple-Well, Multiple-Path Unimolecular Reaction Systems. II. 2-Methylhexyl Free Radicals. *Int. J. Chem. Kinet.* **2001**, *33* (4), 246–261. https://doi.org/10.1002/kin.1018.
- (63) Kelley, K. K. Contributions to the Data on Theoretical Metallurgy. 3. The Free Energies of Vaporization and Vapor Pressures of Inorganic Substances. *Bullletin U.S. Bur. Mines* 1935.
- (64) Gilbert, R. G.; Smith, S. C. *Theory of Unimolecular and Recombination Reactions*; Blackwell Scientific Publications: Oxford, 1990.
- (65) Raabe, G.; Sadus, R. J. Molecular Simulation of the Vapor-Liquid Coexistence of Mercury. *J. Chem. Phys.* **2003**, *119* (13), 6691–6697. https://doi.org/10.1063/1.1605381.
- (66) Nguyen, T. L.; Xue, B. C.; Weston, R. E.; Barker, J. R.; Stanton, J. F. Reaction of HO with CO: Tunneling Is Indeed Important. *J. Phys. Chem. Lett.* **2012**, *3* (11), 1549–1553. https://doi.org/10.1021/jz300443a.
- (67) Natanson, G. A.; Garrett, B. C.; Truong, T. N.; Joseph, T.; Truhlar, D. G. The Definition of Reaction Coordinates for Reaction-Path Dynamics. *J. Chem. Phys.* **1991**, *94* (12), 7875–7892. https://doi.org/10.1063/1.460123.
- (68) Hu, W. P.; Liu, Y. P.; Truhlar, D. G. Variational Transition-State Theory and Semiclassical Tunnelling Calculations with Interpolated Corrections: A New Approach to Interfacing Electronic Structure Theory and Dynamics for Organic Reactions. In *Journal* of the Chemical Society, Faraday Transactions; The Royal Society of Chemistry, 1994; Vol. 90, pp 1715–1725. https://doi.org/10.1039/FT9949001715.
- (69) Fernandez-Ramos, A.; Ellingson, B. A.; Garrett, B. C.; Truhlar, D. G. Variational Transition State Theory with Multidimensional Tunneling. In *Reviews in Computational Chemistry*; Lipkowitz, K. B., Cundari, T. R., Eds.; John Wiley & Sons, Ltd, 2007; pp

- 125–232. https://doi.org/10.1002/9780470116449.ch3.
- (70) Miyoshi, A.; Matsui, H.; Washida, N. Detection and Reactions of the HOCO Radical in Gas Phase. *J. Chem. Phys.* **1994**, *100* (5), 3532–3539. https://doi.org/10.1063/1.466395.
- (71) Bui, T. Q.; Changala, P. B.; Bjork, B. J.; Yu, Q.; Wang, Y.; Stanton, J. F.; Bowman, J.; Ye, J. Spectral Analyses of Trans- and Cis-DOCO Transients via Comb Spectroscopy. *Mol. Phys.* 2018, 116 (23–24), 3710–3717. https://doi.org/10.1080/00268976.2018.1484949.
- (72) Ruscic, B.; Bross, D. H. Active Thermochemical Tables (ATcT) Values Based on Ver. 1.122g of the Thermochemical Network, Argonne National Laboratory; Available at ATcT.Anl.Gov. 2019.
- (73) Ruscic, B.; Pinzon, R. E.; Morton, M. L.; Laszewski, G. von; Bittner, S. J.; Nijsure, S. G.; Amin, K. A.; Minkoff, M.; Wagner, A. F. Introduction to Active Thermochemical Tables: Several "Key" Enthalpies of Formation Revisited. *J. Phys. Chem. A* 2004, 108 (45), 9979–9997.
- (74) Tan, T.; Yang, X.; Ju, Y.; Carter, E. A. Ab Initio Reaction Kinetics of CH₃OC(=O) and CH₂OC(=O)H Radicals. *J. Phys. Chem. B* **2016**, *120* (8), 1590–1600. https://doi.org/10.1021/acs.jpcb.5b07959.
- (75) Slemr, F.; Weigelt, A.; Ebinghaus, R.; Bieser, J.; Brenninkmeijer, C. A. M.; Rauthe-Schöch, A.; Hermann, M.; Martinsson, B. G.; van Velthoven, P.; Bönisch, H.; Neumaier, M.; Zahn, A.; Ziereis, H. Mercury Distribution in the Upper Troposphere and Lowermost Stratosphere According to Measurements by the IAGOS-CARIBIC Observatory: 2014–2016. Atmos. Chem. Phys. 2018, 18 (16), 12329–12343. https://doi.org/10.5194/acp-18-12329-2018.
- (76) Mao, J.; Ren, X.; Brune, W. H.; Olson, J. R.; Crawford, J. H.; Fried, A.; Huey, L. G.; Cohen, R. C.; Heikes, B.; Singh, H. B.; Blake, D. R.; Sachse, G. W.; Diskin, G. S.; Hall, S. R.; Shetter, R. E. Airborne Measurement of OH Reactivity during INTEX-B. *Atmos. Chem. Phys.* 2009, 9 (1), 163–173. https://doi.org/10.5194/acp-9-163-2009.
- (77) Thames, A. B.; Brune, W. H.; Miller, D. O.; Allen, H. M.; Apel, E. C.; Blake, D. R.; Paul Bui, T.; Commane, R.; Crounse, J. D.; Daube, B. C.; Diskin, G. S.; DiGangi, J. P.; Elkins, J. W.; Hall, S. R.; Hanisco, T. F.; Hannun, R. A.; Hintsa, E.; Hornbrook, R. S.; Kim, M. J.; McKain, K.; Moore, F. L.; Nicely, J. M.; Peischl, J.; Ryerson, T. B.; St Clair, J. M.; Sweeney, C.; Teng, A.; Thompson, C. R.; Ullmann, K.; Wennberg, P. O.; Wolfe, G. M. Missing OH Reactivity in the Global Marine Boundary Layer. *Atmos. Chem. Phys* 2020, 20, 4013–4029. https://doi.org/10.5194/acp-20-4013-2020.
- (78) Ferracci, V.; Heimann, I.; Abraham, N. L.; Pyle, J. A.; Archibald, A. T. Global Modelling of the Total OH Reactivity: Investigations on the "Missing" OH Sink and Its Atmospheric Implications. *Atmos. Chem. Phys.* **2018**, *18* (10), 7109–7129. https://doi.org/10.5194/acp-18-7109-2018.
- (79) Tellinghuisen, J.; Ashmore, J. G. Mixed Representations for Diatomic Spectroscopic Data: Application to HgBr. *Chem. Phys. Lett.* **1983**, *102* (1), 10–16.

(80) Shepler, B. C.; Balabanov, N. B.; Peterson, K. A. Hg+Br → HgBr Recombination and Collision-Induced Dissociation Dynamics. *J. Chem. Phys.* **2007**, *127* (16), 164304. https://doi.org/10.1063/1.2777142.